Bioconjugate Chemistry

Article

pubs.acs.org/bc

B6 Peptide-Modified PEG-PLA Nanoparticles for Enhanced Brain Delivery of Neuroprotective Peptide

Zhongyang Liu,[†] Xiaoling Gao,[‡] Ting Kang,[†] Mengyin Jiang,[§] Deyu Miao,[§] Guangzhi Gu,[†] Quanyin Hu,[†] Qingxiang Song,[‡] Lei Yao,[‡] Yifan Tu,[†] Hongzhuan Chen,[‡] Xinguo Jiang,[†] and Jun Chen*[,†]

[†]Key Laboratory of Smart Drug Delivery, Ministry of Education & PLA, School of Pharmacy, Fudan University, 826 Zhangheng Road, Shanghai, 201203, PR China

[‡]Department of Pharmacology, Institute of Medical Sciences, Shanghai Jiaotong University School of Medicine, 280 South Chongqing Road, Shanghai, 200025, PR China

[§]School of Pharmacy, Shandong University of Traditional Chinese Medicine, Jinan, 250355, Shandong People's Republic of China

ABSTRACT: The blood-brain barrier (BBB), which is formed by the brain capillary wall, greatly hinders the development of new drugs for the brain. Over the past decades, among the various receptor-mediated endogenous BBB transport systems, the strategy of using transferrin or anti-transferrin receptor antibodies to facilitate brain drug delivery system is of particular interest. However, the application of large proteins still suffers from the drawbacks including synthesis procedure, stability, and immunological response. Here, we explored a B6 peptide discovered by phage display as a substitute for transferrin, and conjugated it to PEG-PLA nanoparticles (NP) with the aim of enhancing the delivery of neuroprotective drug across the BBB for the treatment of Alzheimer's disease. B6-modified NP (B6-NP) exhibited significantly higher accumulation in brain capillary endothelial cells via lipid raft-mediated and clathrin-mediated endocytosis. In vivo, fluorescently labeled B6-NP exhibited much higher brain accumulation when compared with NP. Administration of B6-NP encapsulated neuroprotective peptide—NAPVSIPQ (NAP)—to Alzheimer's disease mouse models showed excellent amelioration in learning impairments, cholinergic disruption, and loss of hippocampal neurons even at lower dose. These findings together suggested that B6-NP might serve as a promising DDS for facilitating the brain delivery of neuropeptides.

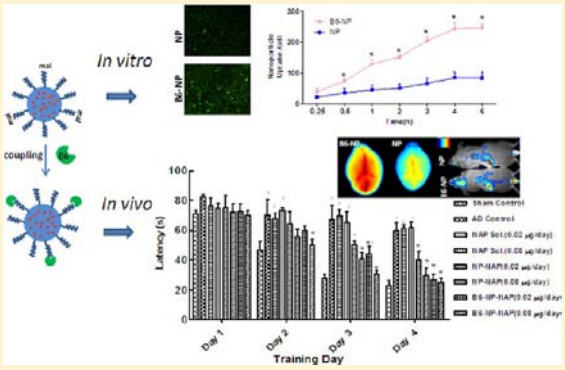

INTRODUCTION

Alzheimer's disease (AD) is the world's most common form of dementia characterized by progressive and specific neuronal and synaptic loss, formation of extracellular senile plaques, and intracellular neurofibrillary tangles in the brain.[1−3] With the population aging, the increasing prevalence of this disease is seen worldwide, which brings pressure not only to the sufferers, but also to their families and even the entire society. Therefore, the development of an effective therapeutic strategy for Alzheimer's disease is of great importance.

A wide variety of neurotrophic proteins and neuropeptides have shown an important neurotrophic role during development and after nerve injury,[4] which brings hope for the treatment of AD. Among them, an octapeptide derived from activity-dependent neuroprotective protein (ADNP)—NAP (NAPVSIPQ)—is identified as a promising neuroprotective agent for AD therapy, and is currently under phase II clinical trials.[5] NAP has shown neuroprotective effects in many *in vivo* and *in vitro* models of neurodegeneration at low concentration (ranging from 10^{-17} to 10^{-10} M) by modulating microtubule organization and stability in neurons.[5−8] *In vitro* in neuronal cell cultures, NAP protected cells against the neurotoxicity induced by β-amyloid, electrical blockade by tetrodotoxin, and oxidative stress by hydrogen peroxide;[4,9,10] and *in vivo* in animal models, NAP protected animals against traumatic brain injury, oxidative stress, and apolipoprotein E-deficiency-associated cholinergic dysfunction and learning/memory impairments.[10−12]

However, due to the nature of peptides, neuroprotective peptides like NAP are very unstable, easy to degrade by enzymes, and present a very short blood half-life *in vivo*.[13] Encapsulation of peptide into the biodegradable poly(ethylene glycol) (PEG)-coated nanoparticles (NP) which possess the ability to cross multiple biological barriers, protect agents from degradation, and extend their circulation half-life might be a promising approach to the delivery of neuroprotective peptides.[14]

Nevertheless, owing to the unique cerebrovascular endothelium sealed with tight junctions, the blood-brain barrier (BBB) severely limits access of therapeutic or diagnostic agents into the brain even incorporating them into NP.[15] The restricted access to the brain is due to a combination of different factors: tight junctions, reduced rate of pinocytosis from the luminal

Received: January 29, 2013
Revised: May 27, 2013
Published: May 29, 2013

side, lack of fenestration, the enzymatic barrier, and the efflux transporter system such as P-glycoproteins.[16] Therefore, to further improve the efficiency and specificity for brain delivery, various strategies to enhance drug delivery across the BBB by targeting biomolecules expressed at the BBB have been studied.[14,16] Among the main target for mediating nanoparticulate delivery, transferrin receptor (TfR), which is highly expressed in BBB endothelial cells, is the most widely studied receptor for BBB targeting[17] and has long been considered among the most promising targets.[18]

Previous studies with brain drug delivery system (DDS) targeting TfR were addressed by incorporating whole transferrin (Tf) protein[19] or anti TfR antibodies.[20] However, the application of large proteins in formulations suffers from the drawbacks including synthesis procedure, stability, and immunological response.[21] On the other hand, characterized as high specificity, low cytotoxicity, and low immunological response, the utility of short peptide targeting system with simplified production process and prolonged storage time is desired. Based on this background, CGHKAKGPRK (denoted as B6), a peptide motif obtained from a previous phage display and showing high affinity to TfR,[22] to our knowledge, may serve as a substitute for Tf protein to mediate brain drug delivery.

It has been demonstrated that poly(ethylene glycol)-poly(lactic acid) block copolymer (PEG-PLA) PEG-PLA nanoparticles remained longer in circulation than those of poly(ethylene glycol)-poly(lactic-*co*-glycolic acid) PEG-PLGA nanoparticles.[23] What's more, prolonged drug release provided by PEG-PLA might be more suitable in the treatment of Alzheimer's disease—a progressive neurodegenerative disorder.[24] Therefore, in our study, we chose PEG-PLA over PEG-PLGA for preparation of the nanoparticles. Using amorphous PDLA to formulate nanoparticles, we studied the potential of B6-conjugated nanoparticles (B6-NP) to deliver a neuroprotective drug across BBB for the treatment of Alzheimer's disease. *In vitro* cellular interaction and *in vivo* brain delivery efficiency of B6-NP were studied. Using NAP as the model drug, neuroprotective effects of the B6-NP formulation was evaluated and compared with unmodified NP and NAP solutions in an AD mice model.

EXPERIMENTAL PROCEDURES

Materials, Cells, and Animals. Methoxy-poly(ethylene glycol) $_{3000}$-poly(lactic acid) $_{34000}$ (MePEG-PLA) and maleimide-poly(ethylene glycol) $_{3400}$-poly(lactic acid) $_{34000}$ (Male-PEG-PLA) were kindly provided by East China University of Science and Technology. B6 peptide (CGHKAKGPRK), with a cysteine on the N-terminal (cys-B6), and NAP (NAPVSIPQ) were synthesized by ChinaPeptides Co., Ltd. (Shanghai, China). DiR (1,1′-dioctadecyl-3,3,3′,3′-tetramethyl indotricarbocyanine iodide), a near-infrared dye, was offered by Biotium (Hayward, CA). Coumarin-6, β-amyloid$_{1-40}$ (Aβ_{1-40}), and ibotenic acid (IBO) were purchased from Sigma-Aldrich (Saint Louis, MO). DAPI (4,6-diamidino-2-phenylindole) was obtained from Molecular Probes (Eugene, OR, USA) and BCA protein assay kit from Pierce (Rockford, IL, USA). Quantity Protein assay kits and AChE and ChAT activity assay kits were purchased from Nanjing Jiancheng Bioengineering Institute (Nanjing, China). All the other materials were of HPLC or analytical reagent grades and used without further purification.

Plastic cell culture dishes, plates, and flasks were obtained from Corning Incorporation (Lowell, MA); Dulbecco's Modified Eagle Medium (high glucose) cell culture medium, penicillin−streptomycin, fetal bovine serum (FBS), and 0.25% (w/v) trypsin solution were from Gibco BRL (Carlsbad, CA, USA). Double-distilled water was prepared using a Millipore Simplicity System (Millipore, Bedford, USA).

Immortalized murine microvascular endothelial bEnd.3 cells were provided by Cell Institute of Chinese Academy of Sciences (Shanghai, China) and cultured in DMEM supplemented with 10% FBS, 100 U/mL penicillin and 100 μg/mL streptomycin at 37 °C in a humidified atmosphere containing 5% CO_2.

Male ICR mice (4−5 weeks, 20 ± 2 g) and Balb/C nude mice (20−22 g) were obtained from BK Lab Animal Ltd. (Shanghai, China) and maintained at 25 ± 1 °C with free access to food and water. The protocol of animal experiments was approved by the Animal Experimentation Ethics Committee of Fudan University.

Preparation of Nanoparticles. Unmodified nanoparticles (NP) loaded with coumarin-6, NAP, or DiR were prepared using an emulsion/solvent evaporation technique.[25] For coumarin-6-loaded or DiR-loaded NP, 50 μL of deionized water (internal aqueous phase) was added to 1 mL dichloromethane containing 22.5 mg MePEG-PLA, 2.5 mg Male-PEG-PLA, and 0.1% (w/w) of coumarin-6 or 1% (w/w) DiR (oil phase); the w/o primary emulsion was produced by sonication (160 W, 30 s) on ice using a probe sonicator (Ningbo Scientz Biotechnology Co. Ltd., China). The primary emulsion was then re-emulsified with the external aqueous phase containing 2 mL of 1% sodium cholate solution by sonication (220 W, 30 s) on ice. Afterward, to solidify the double emulsion droplets, the w/o/w emulsion was further diluted into 8 mL of a 0.5% aqueous sodium cholate solution and then stirred for 5 min at room temperature. After that, the emulsion was applied to a ZX-98 rotavapor (Shanghai Institute of Organic Chemistry, China) to remove the organic solvent and concentrated by centrifugation at 15000 rpm for 45 min using a TJ-25 centrifuge (Beckman Counter, USA) at 4 °C. After discarding the supernatant, the nanoparticles were resuspended in 2 mL HEPES buffer (pH 7.0) and then subjected to a 1.5 × 20 cm Sepharose CL-4B column (Pharmacia Biotech, Inc., Sweden) to remove the unencapsulated agents.

The NAP-load NP (NP-NAP) was prepared with the same procedure except using 50 μL of NAP solution (25 mg/mL) as the inner phase of the primary emulsion.

B6-functionalized NPs (B6-NP) were prepared via a maleimide−thiol coupling reaction at room temperature for 8 h. The products were then subjected to a 1.5 × 20 cm sepharose CL-4B column and eluted with 0.01 M HEPES buffer (pH 7.0) to remove the unconjugated peptides.

Characterization of the Nanoparticles. The morphology of nanoparticles was characterized under a transmission electron microscope (TEM) (H-600, Hitachi, Japan) following negative staining with sodium phosphotung state solution (2%, w/v). The particle size, size distribution, and zeta potential were determined by dynamic light scattering (DLS) using Malvern Zetasizer Nano ZS (Malvern, UK).

Encapsulation Efficiency, Drug Loading Capacity and *in Vitro* Drug Release Profiles. For determining the encapsulation efficiency (EE) and loading capacity (LC) of NAP-loaded B6-NP (B6-NP-NAP), the NAP was released from the NPs following the addition of acetonitrile. After

precipitating the polymers with 0.1% (v/v) trifluoroacetic acid, the samples were centrifuged at 12000 rpm for 10 min. The concentration of NAP in supernatant was determined via an HPLC analysis using 0.1% trifluoroacetic acid in acetonitrile:0.1% trifluoroacetic acid in water 15:85 as the mobile phase at the flow rate 1 mL/min and detection wavelength 225 nm). EE% and LC% were calculated as indicated below ($n = 3$):

$$\mathrm{LC}(\%) = \frac{\text{amount of NAP in nanoparticles}}{\text{nanoparticles weight}} \times 100\%$$

$$\mathrm{EE}(\%) = \frac{\text{amount of NAP in nanoparticles}}{\text{total amount of NAP added initially}} \times 100\%$$

To determine the release of NAP from nanoparticles, both NAP-loaded NP and B6-NP (nanoparticles concentration, 2.5 mg/mL) were dispersed in deionized water, and then divided equally into 54 shares (0.5 mL/share), respectively. After incubating at 37 °C, at each predetermined time point (0 h, 0.5 h, 1 h, 2 h, 4 h, 8 h, 12 h, 24 h, and 48 h, $n = 3$), the samples were collected and centrifuged at 17500 rpm for 20 min, followed by the supernatants carefully discarded and the precipitates resuspended in 30 μL acetonitrile. 60 μL 0.1% (v/v) trifluoroacetic acid was then added to each sample of resuspended products, and the concentrations of NAP entrapped in NP or B6-NP at each time point were measured with the HPLC method as described above. The cumulative release percentage (CR) of NAP from NP or B6-NP at each time intervals was calculated as indicated below:

$$\mathrm{CR}(\%) = \left(1 - \frac{\text{amount of NAP in precipitate}}{\text{amount of NAP in the nanoparticles initially}}\right) \times 100\%$$

X-ray Photoelectron Spectroscopy (XPS), B6 Conjugation Efficiency, and B6 Density on Nanoparticle Surface. In order to determine the surface composition of NP and B6-NP, the samples were lyophilized using an ALPHA 2−4 Freeze-Dryer (0.070 Mbar Vakuum, −80 °C Martin Christ, Germany) and subjected to XPS analysis via a RBD upgraded PHI-5000C ESCA system (Perkin-Elmer).

The B6 conjugation efficiency (CE) was measured via a BCA assay: triplicate wells (96-well plate) of aliquots of either B6-NP or NP (dissolved in PBS pH 7.4) were treated following the manufacturer's instructions and then subjected to absorption analysis under a microplate reader (Thermo Multiskan MK3, USA) at 562 nm. The CE calculation formula is as follows:

$$\mathrm{CE}(\%) = \frac{\text{amount of B6 conjugated to the nanoparticle surface}}{\text{total amount of B6 added}} \times 100\%$$

The B6 surface density was calculated by dividing the number of B6 molecules by the calculated average number (n) of nanoparticles using the methods described previously:[26] $n = 6m/(\pi \times D^3 \times \rho)$ (m, the nanoparticle weight; D, the number-based mean nanoparticle diameter determined by DLS; ρ, the nanoparticle weight per volume unit (density), estimated to be 1.1 g/cm^3).[27]

Cellular Association/Uptake of Coumarin-6-Labeled NPs. For qualitative cellular association experiment, bEnd.3 cells were seeded into 24-well plates at the density of 4×10^4 cells per well one day prior to study. The cells were then incubated with different concentrations of coumarin-6-labeled NPs for 1 h. After that, the cells were washed three times with PBS, and fixed with 4% formaldehyde for 10 min. Following cell nuclear staining with 100 ng/mL DAPI for 10 min, the cells were observed under a fluorescent microscope (Olympus, Japan).

For quantitative cellular uptake experiment, a previously described High Content Cell Analysis System (HCS) [28] was applied for analysis. Briefly, after plating on a 96-well plate at the density of 5×10^3 cells/well for 24 h, the bEnd.3 cells were then incubated with courmarin-6-loaded B6-NP and NP (25−600 μg/mL) for 1 h at 4 and 37 °C, respectively. For nucleic acid staining, the cells, protected from light, were fixed and stained with 10 μg/mL Hochest 33258 (Pentahydrate (bis-Benzimide), a nucleic acid stain) at room temperature for 10 min. For determining the level of cellular internalized nanoparticles, the cells were incubated with trypan blue (Beyotime Institute of Biotechnology) to quench the fluorescent signals from the uninternalized ones, and then subjected to a KineticScan HCS Reader (version 3.1, Cellomics Inc., Pittsburgh, PA, USA). To study the effects of incubation time on nanoparticle uptake, the cells were incubated with 200 μg/mL nanoparticles for 0.5 to 6 h.

In the inhibition experiment, seeded bEnd.3 cells (5×10^3 cells/well, 96-well plate, for 24 h) were incubated with 10 μg/mL chlorpromazine, 4 μg/mL colchicines, 10 μg/mL cyto-D, 5 μg/mL BFA, 5 μg/mL filipin, 10 mM NaN_3 + 50 mM deoxyglucose, 2.5 mM methyl-β-cyclodextrin (M-β-CD), 200 nM monensin, 20 μM nocodazole, or 100 μg B6 peptiede for 30 min, respectively. Quantitative analysis of the cellular uptake following the inhibitor treatments was performed as mentioned above and compared with that of the noninhibited control.

***In Vitro* Cell Viability Assay.** Cell Counting Kit-8 (CCK-8) assay was used to evaluate the effect of B6-NP-NAP or NP-NAP on the viability of bEnd.3 cells. The cells were seeded into 96-well plates at the density of 5×10^3 cells per well and cultured for 24 h. The medium was then replaced with serum-free DMEM containing B6-NP-NAP or NP-NAP for 24 and 48 h, respectively, at the NP concentration ranging from 0 to 2 mg/mL. After incubating for 24 and 48 h, respectively, the medium was removed and replenished with fresh serum-free DMEM with 10 μL CCK-8 solution added to each well. One hour later, the absorbance of each well was measured via a microplate reader at 450 nm and the viability of bEnd.3 cells was reflected by the percentage of absorbance of sample groups in comparison with that of the NPs-free control.

***In Vivo* Real-Time Imaging.** In order to study the *in vivo* real-time distribution of NPs, near-infrared dye DiR was used as the probe. The DiR-loaded NP or B6-NP was injected into the tail vein of BALB/c nude mice at an equal dose of DiR (1 mg/kg). The fluorescent images were detected by Maestro *in vivo* imaging system (CRi, MA, USA) at predetermined time points. One hour after injection, brains and other main organs were harvested, washed with saline, and visualized for relative accumulation comparison.

$A\beta_{1-40}$ and IBO Coinjection Model. Male ICR mice (4−5 weeks, 20 ± 2 g) were used in the study and randomly divided into eight groups ($n = 8$). Before surgery, $A\beta_{1-40}$ (preaggregated at 37 °C for 7 days, 2 μg/μL) and IBO (2 μg/μL) were mixed to a final concentration of $A\beta_{1-40}$ 1 μg/μL and IBO 0.5 μg/μL in saline. The mice were anaesthetized with

dx.doi.org/10.1021/bc400055h | Bioconjugate Chem. 2013, 24, 997−1007

chloral hydrate and then fixed in a stereotaxic apparatus equipped with a mouse adaptor. Five microliters of the mixture of $A\beta_{1-40}$ and IBO or the same volume of saline were bilaterally injected in the dorsal hippocampus with a Hamilton microsyringe over 6 min.

Morris Water Maze (MWM) Task. Four days after the surgery, each group received daily administration of the formulations for 30 consecutive days: saline for AD controls and sham controls; NAP solutions (NAP, 0.02 μg/mouse/day and 0.08 μg/mouse/day, respectively); NP-NAP (NAP, 0.02 μg/mouse/day and 0.08 μg/mouse/day, respectively); or B6-NP-NAP (NAP, 0.02 μg/mouse/day and 0.08 μg/mouse/day, respectively). MWM test was carried out from the 30th day.

The MWM device consists of a large circular pool (120 cm diameter and 50 cm depth) filled with opaque water at a temperature of 25 ± 1 °C in which a 9-cm escape platform is hidden. [29] A four-day training session or a probe trail was carried out 1 h following drug administration. During the first four-day training, the animals were placed into the tank from four starting points in a random manner with 90 s latency to reach the platform. Each mouse was allowed to rest for 15 s on the condition of locating the platform within 90 s. If it failed, animal had to be put on the platform and stay for 15 s. Swimming trajectories were recorded and analyzed using a computerized video-tracking system. On the fifth day, a single probe trail was performed with the platform removed and the mouse allowed to swim freely for 60 s from two starting points far away from the platform. The percentage of time spent in targeted quadrant of the MWM and the number of crossings over the previous platform position were recorded.

AChE Activity and ChAT Activity in Mice Hippocampus. After the MWM task, the mice (n = 5) were sacrificed, with the AChE and ChAT activity in mice hippocampus determined spectrophotometrically using the Quantity Protein assay kit according to the manufacturer's protocols.[30]

Histology. At the end of the behavioral studies, the mice (n = 3) were anaesthetized with chloral hydrate, and transcardially perfused with saline and 4% paraformaldehyde solution. The whole brains were harvested and further fixed in 4% paraformaldehyde solution, embedded in paraffin, sectioned at 5 μm, and stained with hematoxylin/eosin (HE) following standard protocol.

Statistical Analysis. All the data were presented as mean ± SD unless otherwise indicated. Unpaired Student's t test was used for comparison between two groups and one-way ANOVA with Bonferroni tests for multiple-group analysis. Statistical significance was defined as $p < 0.05$.

RESULTS

Characterization of the Nanoparticles. The physical characterization of coumarin-6/DiR/NAP-loaded nanoparticles was shown in Table 1. The average particle sizes of NP and B6-NP were between 100 and 120 nm with acceptably polydispersity indexes (PI < 0.25). The B6 conjugation slightly increased the particle size. Both nanoparticles were spherical and uniform under transmission electron microscope (Figure 1).

The existence of B6 on the surface of B6-NP was confirmed by XPS analysis which showed 1.05% nitrogen on the B6-NP surface but none on the surface of unconjugated NP. Under our experimental conditions (molar ratio of maleimide-PEG-PLA to B6 1:1 and incubation time for conjugation reaction 8 h), the B6 peptide conjugation efficiency was 42.7 ± 3.6%, and its density on the nanoparticle surface was around 355.

Table 1. Characterization of Coumarin-6/DiR/NAP-Loaded NP and B6-NP[a]

formulation	vesicle size (nm)	PI	zeta potential (mV)
coumarin-6-NP	103.3 ± 4.9	0.15 ± 0.024	−24.35 ± 0.89
coumarin-6-B6-NP	119.5 ± 5.2	0.20 ± 0.039	−22.18 ± 1.12
DiR-NP	104.2 ± 5.5	0.11 ± 0.021	−25.28 ± 1.57
DiR-B6-NP	117.7 ± 6.5	0.23 ± 0.048	−21.84 ± 0.79
NP-NAP	106.9 ± 5.8	0.12 ± 0.034	−24.47 ± 1.01
B6-NP-NAP	118.3 ± 7.8	0.25 ± 0.038	−22.65 ± 0.85

[a]Data are represented with mean ± SD (n = 3).

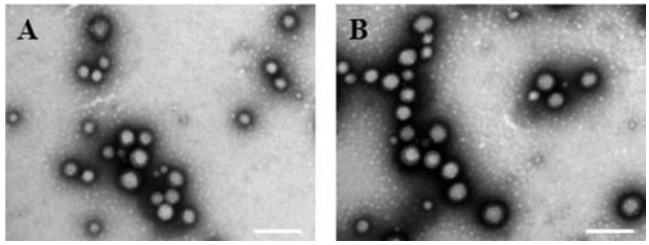

Figure 1. Transmission electron micrographs of (A) NP and (B) B6-NP. Bar, 200 nm.

The EE and LC of NP-NAP and B6-NP-NAP were 56.82 ± 4.20%, 51.16 ± 3.51%, and 0.65 ± 0.021%, 0.57 ± 0.023%, respectively.

In vitro release data showed that NAP-loaded NP and B6-NP (Figure 2) displayed a similar release pattern in deionized water with approximately 20% NAP released from both NP and B6-NP during 48 h incubation.

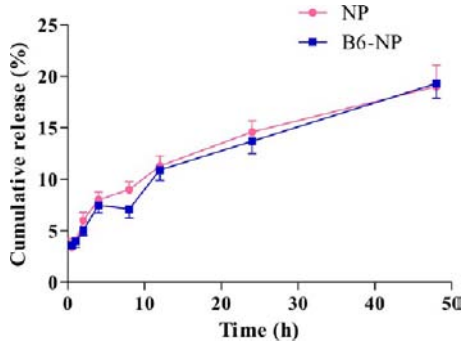

Figure 2. NAP release profiles from NP-NAP, B6-NP-NAP in deionized water at 37 °C.

Cellular Association/Uptake of Coumarin-6-Labeled NPs. Qualitative cellular association experiments were performed via fluorescent microscopy analysis using coumarin-6 as the fluorescent probe. As shown in Figure 3, the cellular associated fluorescence intensity of B6-NP was significantly higher than that of NP.

These results were further confirmed by quantitative cellular uptake analysis (Figure 4A) at both 37 and 4 °C (at 37 °C, about 2.65, 2.49, 2.46, 2.53, and 2.33 times higher than that of NP at the concentration of 100, 200, 300, 400, and 600 μg/mL, respectively; and at 4 °C about 2.75, 2.55, 2.91, 2.87, and 2.67 times higher than that of NP at the concentration of 100, 200, 300, 400, and 600 μg/mL, respectively). A time-dependent

dx.doi.org/10.1021/bc400055h | Bioconjugate Chem. 2013, 24, 997−1007

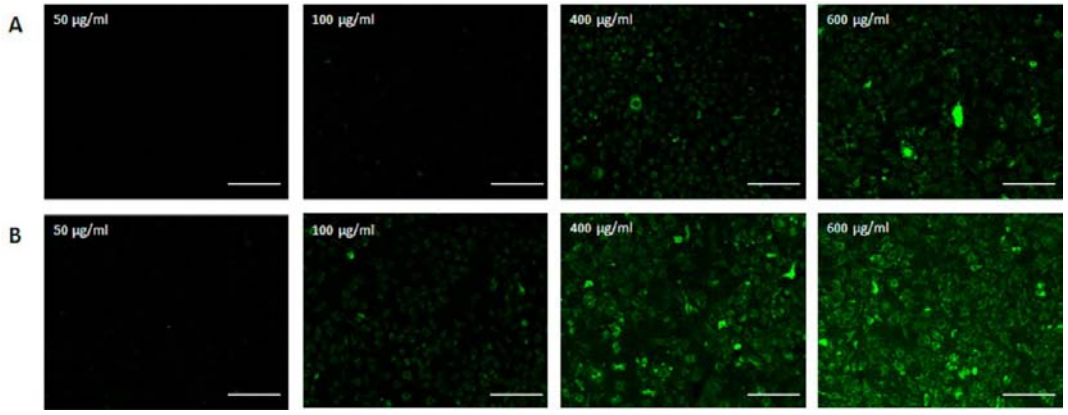

Figure 3. Cellular association of NP (A) and B6-NP (B) in bEnd.3 cells under a fluorescence microscope at coumarin-6 concentration points (50, 100, 400, 600 ng/mL, respectively) following 1 h incubation at 37 °C. Bar, 50 mm.

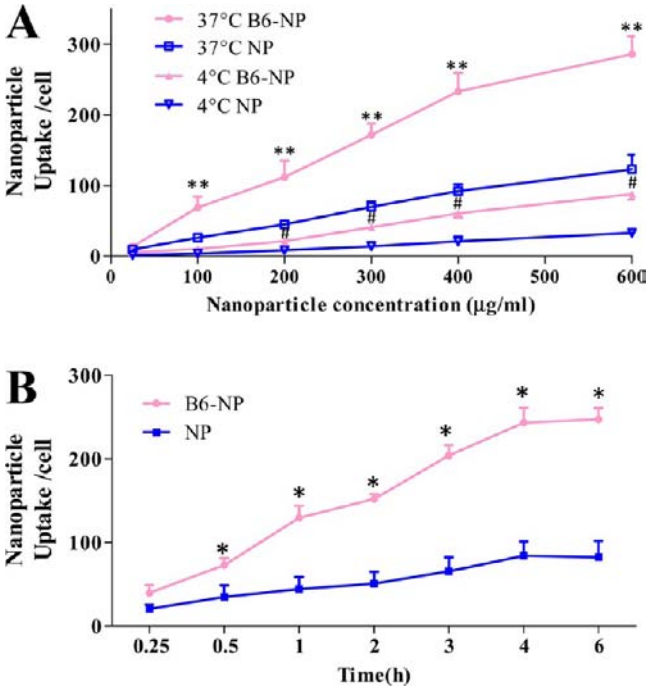

Figure 4. Temperature and time-dependent cellular uptake of coumarin-6-loaded nanoparticles in bEnd.3 cells. (A) The cells were incubated with B6-NP and NP (25−600 μg/mL) for 1 h at 37 and 4 °C, respectively. (B) The cells were incubated with B6-NP and NP (200 μg/mL) at 37 °C for 0.25, 0.5, 1, 2, 3, 4, and 6 h, respectively. * $p < 0.05$, ** $p < 0.01$ significantly different from that of NP at 37 °C; # $p < 0.05$, significantly different from that of NP at 4 °C.

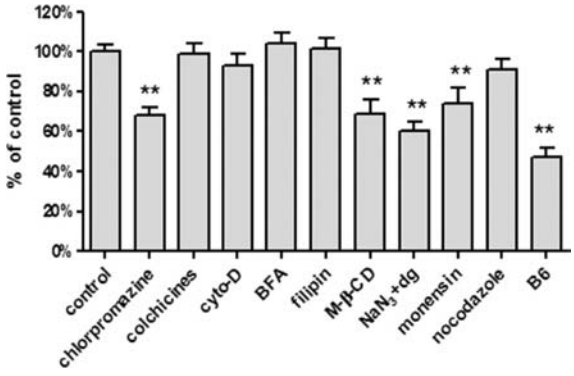

Figure 5. Cellular uptake of coumarin-6-labeled B6-NP in bEnd.3 cells in the presence of chlorpromazine, colchicines, cyto-D, BFA, filipin, NaN_3 together with deoxyglucose, M-β-CD, monensin, nocodazole, and B6, respectively. Fluorescence intensity of coumarin-6 in the noninhibited cells, representing the control internalized amount of coumarin-6-labeled B6-NP, *$p < 0.05$, **$p < 0.01$ significantly different from the noninhibited control ($n = 3$).

pattern in cellular uptake was achieved by both NP and B6-NP although the uptake of B6-NP was higher than that of NP (Figure 4B).

In the inhibition experiment, as shown in Figure 5, the treatment of chlorpromazine, M-β-CD, NaN_3 + dg, and monesin exhibited a significant inhibition in cellular uptake of B6-NP when compared with the noninhibited control. In addition, significant inhibition in cellular uptake of B6-NP was also observed following preincubated with excess B6.

***In Vitro* Cell Viability Assay.** *In vitro* cell viability analysis was performed following B6-NP-NAP/NP-NAP treatment in bEnd.3 cells after 24 and 48 h incubation at 37 °C via a CCK-8 assay. As shown in Figure 6, no significant cytotoxicity of the formulations was detected at any of the given concentrations ($P > 0.05$).

***In Vivo* Real-Time Imaging.** The B6 peptide brain targeting ability was studied via a real-time imaging system. After the DiR-labeled NPs were injected through the tail vein, according to Figure 7A, it was found that the fluorescence signals of B6-NP remaining in brain were much higher than that of NP at all time points from 0.5 to 12 h post administration. One hour post administration, fluorescence intensity of B6-NP from the harvested brain was also found to be higher than of NP (Figure 7B).

Behavioral Analysis of $A\beta_{1-40}$ and IBO Coinjected Mice. Classic MWM task was used to evaluate the spatial learning and memory of the tested mice. As shown in Figure 8A, all groups of mice showed improvement in finding the hidden platform over the four day training session. However, the AD control group exhibited a significantly longer latency ($p < 0.05$) than that of sham control group (on day 2, 3, 4); a dose of 0.08 μg/mouse/day (NAP) of B6-NP-NAP (on day 2, 3, 4); a dose of 0.02 μg/mouse/day (NAP) of B6-NP-NAP (on day 3, 4); a dose of 0.08 μg/mouse/day (NAP) of NP-NAP (on day 3, 4); and a dose of 0.02 μg/mouse/day (NAP) of NP-NAP (on day 4), respectively. A two-way ANOVA analysis performed on a four day training session revealed significant

dx.doi.org/10.1021/bc400055h | *Bioconjugate Chem.* 2013, 24, 997−1007

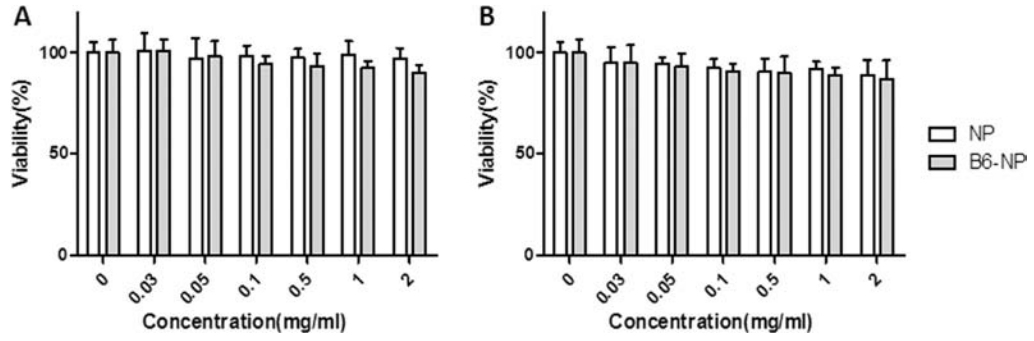

Figure 6. *In vitro* cell viability of NP-NAP and B6-NP-NAP incubated with bEnd.3 cells for (A) 24 h and (B) 48 h at 37 °C.

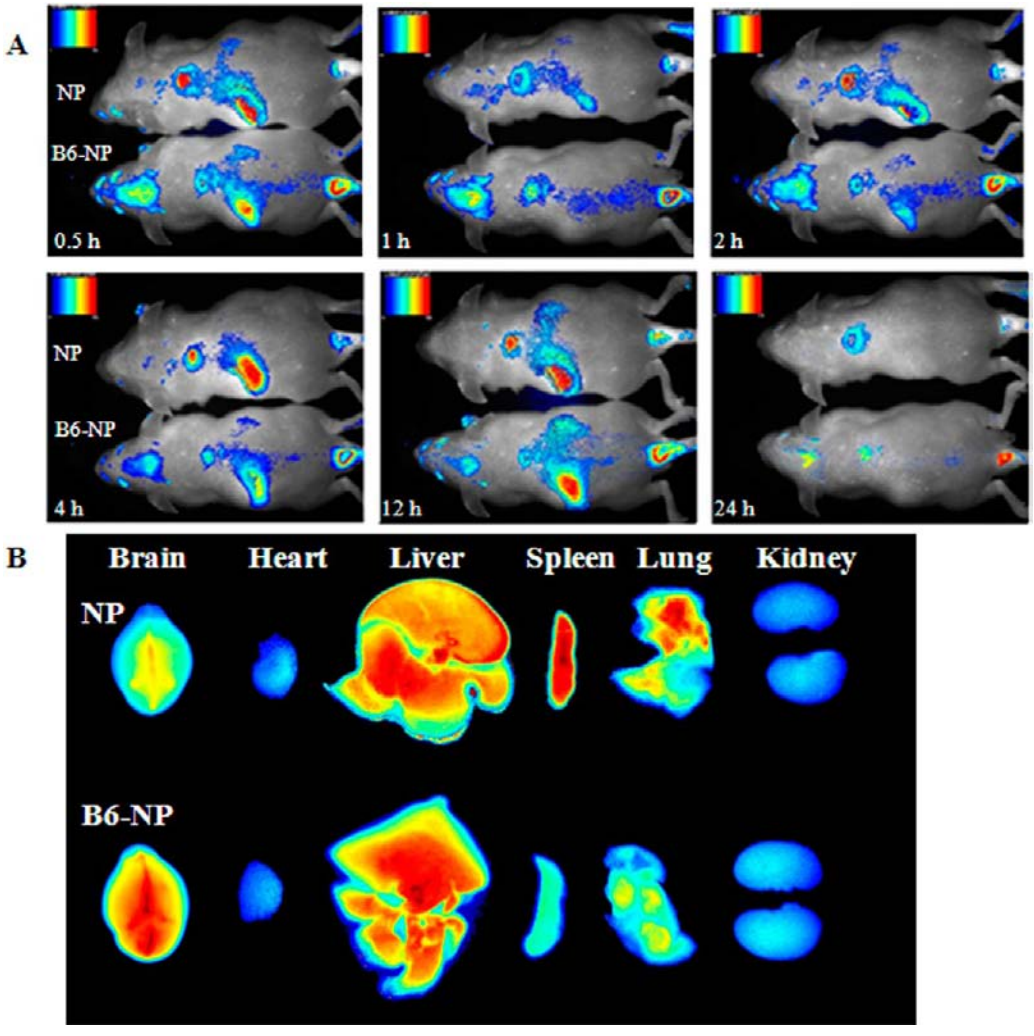

Figure 7. (A) Distribution and retention of B6-NP or NP in the nude mice following tail vein intravenous administration. (B) Distribution of B6-NP or NP in brain and main organs 1 h after administration.

treatment and dose effects for latency in the MWM task: compared at the same NAP administration dose, the reduction in latency followed the order of B6-NP-NAP > NP-NAP; and the reduction in latency also followed a dose response pattern. The further probe trial results (Figure 8B,C) were consistent with these findings. Both the number of times crossing the area where the platform had been located and the percentage of time spent in the target quadrant confirmed the treatment- and dose-dependent manner among the NP-NAP groups and B6-NP-NAP groups. On the other hand, when compared with the AD control group, daily administration of NAP solution groups showed no significant difference.

AChE and ChAT Activity in Mice Hippocampus. To further investigate the neuroprotective effects of B6-NP on AD model mice, we determined the AChE and ChAT activity in model mouse hippocampus after the MWM task. The recognition memory improvement was reflected by the inhibition of ChAT and increase of AChE activity in mice with lesions induced by intracerebroventricular coinjection with $A\beta_{1-40}$ and IBO. As shown in Figure 9A, the activity of AChE

dx.doi.org/10.1021/bc400055h | *Bioconjugate Chem.* 2013, 24, 997−1007

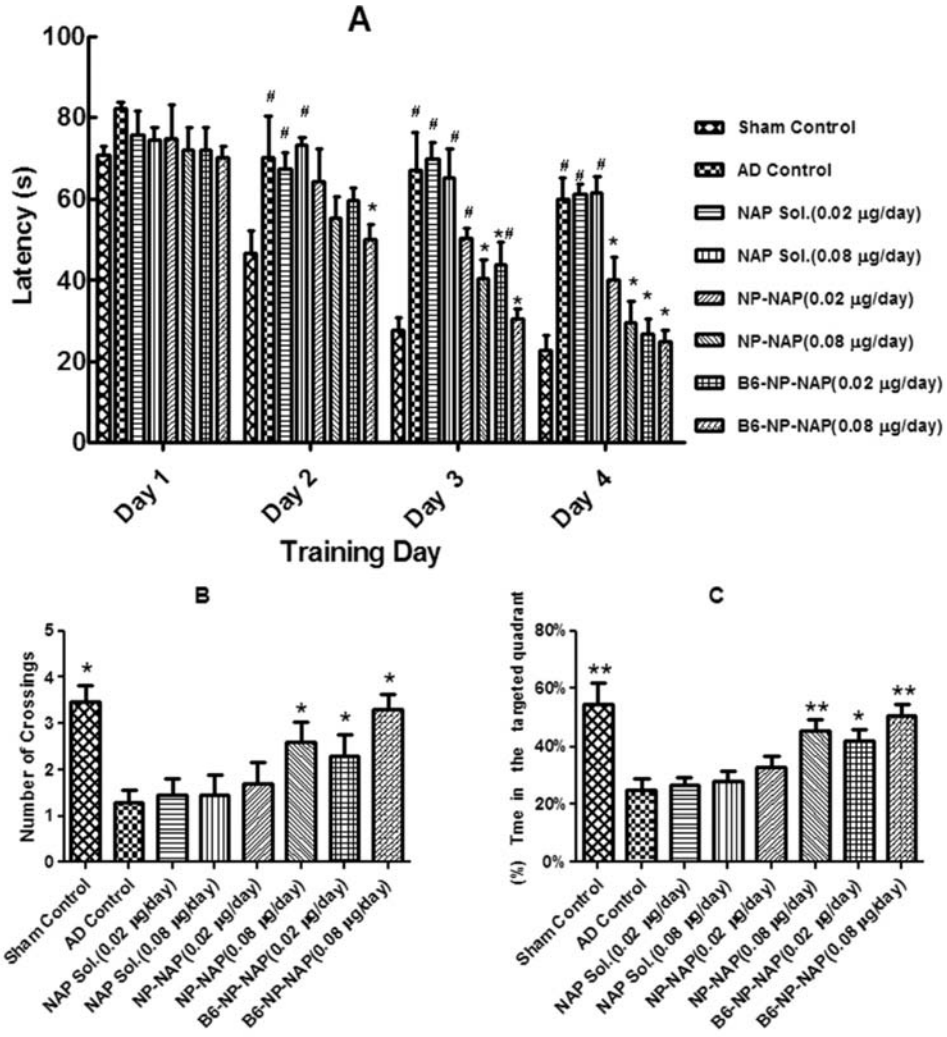

Figure 8. (A) Neuroprotection effects of NAP solution, NP-NAP, and B6-NP-NAP on the impairment of water maze learning in mice with lesions induced by intracerebroventricular coinjection with $A\beta_{1-40}$ and IBO. Training began after 34 days of recovery and daily drug application. Data represented the mean ± SD. (B) The number of crossings of the removed platform area in the probe test: Day 5 of testing, a spatial probe test performed with the platform removed. The animals were allowed to swim for 60 s, and the mean number of times the animals crossed the area where the platform had been located was recorded. Data represented the mean ± SD. (C) The percentage of (%) time in the targeted quadrant where the platform had been located. Data represented the mean ± SD (n = 8). * $p < 0.05$, ** $p < 0.01$ significantly different from AD control; # $p < 0.05$, significantly different from sham control. Sham control, given saline instead of $A\beta_{1-40}$ and IBO and received daily applied saline; AD control, daily applied saline; NAP Sol. (0.02 μg/day), tail vein administration of NAP solution at the dose of 0.02 μg/mouse/day NAP; NAP Sol. (0.08 μg/day), tail vein administration of NAP solution at the dose of 0.08 μg/mouse/day NAP; NP-NAP (0.02 μg/day), tail vein administration of NP-NAP at the dose of 0.02 μg/mouse/day NAP; NP-NAP (0.08 μg/day), tail vein administration of NP-NAP at the dose of 0.08 μg/mouse/day NAP; B6-NP-NAP (0.02 μg/day), tail vein administration of B6-NP-NAP at the dose of 0.02 μg/mouse/day NAP; B6-NP-NAP(0.08 μg/day), tail vein administration of B6-NP-NAP at the dose of 0.08 μg/mouse/day NAP.

decreased to the normal level after injection of NP-NAP (0.08 μg/day) and B6-NP-NAP (0.02 μg/day and 0.08 μg/day). The ChAT activity exhibited an opposing tendency (Figure 9B), with the NP-NAP (0.08 μg/day) group and B6-NP-NAP groups reversed the reduced activity of ChAT.

Histology. HE staining was conducted to evaluate the amelioration of the formulations on neuronal damage in the hippocampal area (Figure 10). Compared with sham control, AD control animals showed obvious damage in the hippocampus where apoptotic cells with dense nuclei or karyolysis were observed (Figure 10A,B). The reduction of cell numbers in the CA1 region of hippocampus was also observed. Compared with AD control group, pathological damage was slightly ameliorated following the NAP treatments in the following order: 0.02 μg/mouse/d NAP solution group < 0.08 μg/mouse/d NAP solution group < 0.02 μg/mouse/d NP-NAP < 0.08 μg/mouse/d NP-NAP group. In contrast, significant improvement was observed in those mice treated with B6-NP-NAP and no obvious morphological damage was detected.

DISCUSSION

AD and related neurodegenerative disorders are among the principal debilitating conditions of the 21st century.[31] However, to better affect disease outcomes, an efficient drug delivery system to the central nervous system (CNS) thus penetrating the BBB remains a challenging clinical problem.

Tight intercellular junctions, low pinocytic potential, expression of outwardly drug efflux transporters, and high levels of drug metabolizing enzymes: all these factors limit the BBB permeability of neuroactive agents, representing a major

dx.doi.org/10.1021/bc400055h | Bioconjugate Chem. 2013, 24, 997−1007

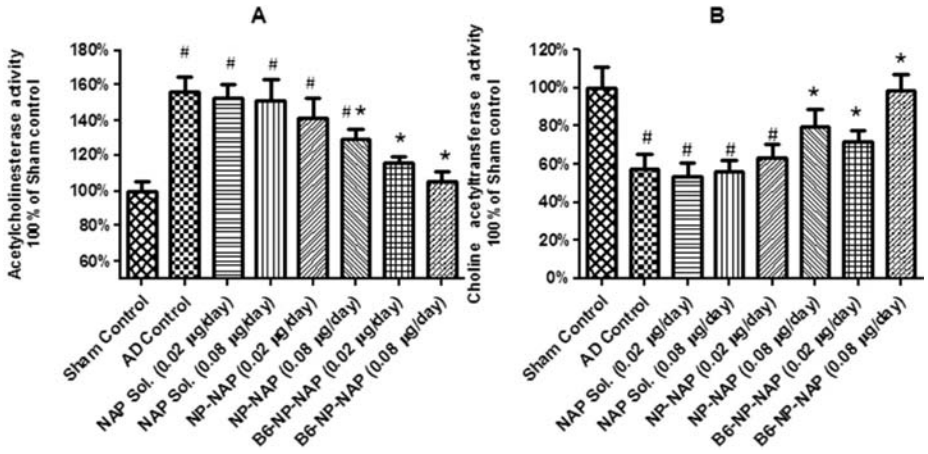

Figure 9. Application of B6-NP-NAP nanoparticles prevented activation of (A) AchE and inhibition of (B) ChAT activity in the hippocampus of mice intracerebroventricular coinjected with Aβ_{1-40} and IBO. Results were calibrated against sham control (100%). Data represented the mean ± SD (n = 5). * $p < 0.05$, significantly different from AD control; # $p < 0.05$, significantly different from sham control.

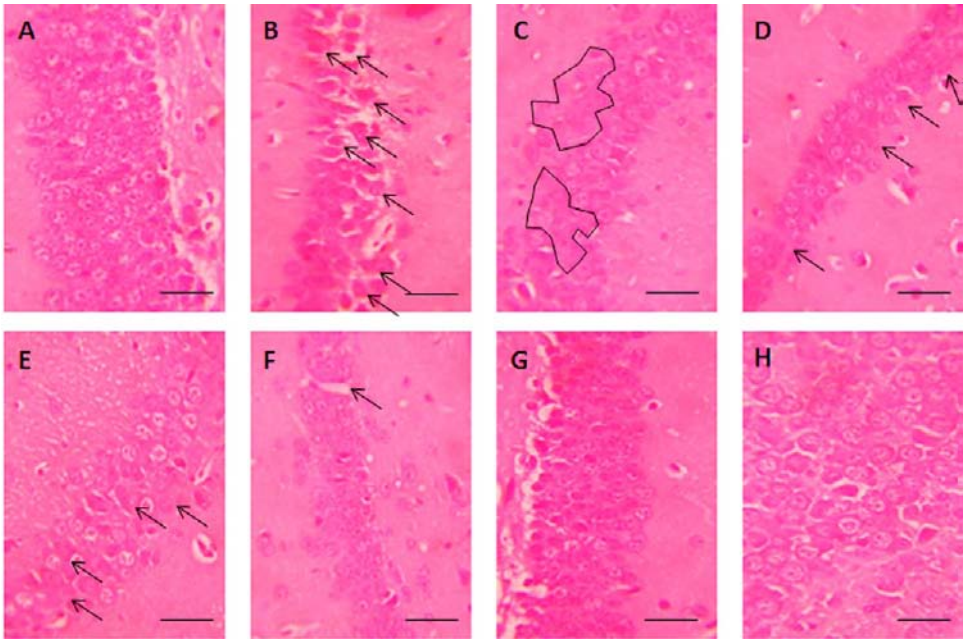

Figure 10. Representative images of HE staining in the right hippocampus CA1 region of the Aβ_{1-40} and IBO coinjected mice: (A) sham control; (B) AD control; (C) NAP Sol. (0.02 μg/day); (D) NAP Sol. (0.08 μg/day); (E) NP-NAP (0.02 μg/day); (F) NP-NAP (0.08 μg/day); (G) B6-NP-NAP (0.02 μg/day); and (H) B6-NP-NAP (0.08 μg/day). Bar, 25 μm. Numerous neuronal cells in the AD control animals were damaged following the coinjection of Aβ_{1-40} and IBO. B6-NP-NAP treatment significantly reduced the number of damaged neuronal cells. Arrows show neuronal damage (apoptotic cells with dense nuclei or karyolysis, and neuronal cell loss) in hippocampus in B, D, E, and F. Black polygon shows neuronal damage in hippocampus in C.

bottleneck in the development of efficacious and safe treatment of CNS disorders.[31] To overcome these difficulties, on the basis of the investigations conducted so far, with the help of certain endogeneous proteins such as Tf, insulin, lactoferrin (Lf),[32] receptor-mediated transport (RMT) traverses BBB and gains access to intracerebral drug delivery. The discovery of RMT also led to development of other BBB transport systems: genetically engineered fusion antibody such as HIRMAb-AV,[33,34] cTfRMAb-AV,[35] a trifunctional fusion antibody that binds (1) the human insulin receptor, (2) the Aβ fibril, and (3) the Fc receptor,[36] and HIRMAb-IDUA fusion protein.[37] Among them, Tf, the ligand of TfR, has been widely studied to facilitate the brain delivery of small molecular drugs,[38] proteins,[39] and gene materials.[40] However, the usage of large proteins as Tf in formulations still has drawbacks including synthesis procedure, stability, and immunological response. Therefore, with B6 peptide obtained from phage display, which targets TfR that presents in the brain capillary endothelia and also in neurons, we constructed a short peptide-modified NP as a safe and efficient DDS for the treatment of AD.[41,42] Using NAP as a model drug, we evaluated the efficacy of B6-NP-NAP for neuroprotection in AD animal model following i.v. administration.

From the TEM photos and DLS measurements, we find that NP was well accommodated in solution with an average diameter of around 100 nm. Its size increased to around 120 nm after B6 conjugation, resulting a favorable size distribution for brain drug delivery. The BCA Protein Quantitation results

in line with XPS analysis confirmed the presence of B6 on the surface of B6-NP.

The stability of the coumarin-6/DiR-labeled NP was examined using *in vitro* release studies conducted in pH 4.0 and pH 7.4, showing that almost all the fluorescent probes remained in NPs during the experimental period (data not shown). This suggests that the relatively stable coumarin-6-labeled NP and DiR-labeled NP could represent the fate of NP both *in vitro* and *in vivo*. Besides, the *in vitro* NAP release results suggest that most of the NAP encapsulated in NP or B6 modified NP may remain in NP in physiological environment following administration, and thus a certain amount of it could be delivered into the CNS following tail vein injection.

To investigate the cellular association of B6-NP, bEnd.3 cells, a brain capillary endothelial cell line was used as the cell model that can form a layer with BBB properties: form tight junction between the cells, express gamma-glutamyl-transpeptidase (gamma-GTP) and P-glycoprotein (P-gp), and restrict paracellular transport.[43] The fluorescent microscope images suggested that B6 modification effectively enhanced cellular association of NP. To further explore the difference in cellular uptake of B6-NP and NP in bEnd.3 cells, quantitative experiments were performed at different concentration, temperature, and time period. The observed time, concentration, and temperature-dependent cellular uptake pattern of both B6-NP and NP indicate an active endocytotic process.

To further elucidate the internalization pattern of B6-NP, we conducted a quantitative study exploring the effects of several different inhibitors on the cellular uptake of B6-NP. It was found that energy-depletion agent—NaN_3 + deoxyglucose—significantly reduced ($p < 0.05$) the cellular uptake of B6-NP (Figure 5), consistent with the reduced cellular uptake of B6-NP at 4 °C (Figure 4A), indicating that an energy-dependent process played an important role in the cellular interaction with B6-NP. It was also found that clathrin-mediated endocytosis pathway inhibitor—chlorpromazine—significantly reduced the cellular uptake of B6-NP compared with that of the noninhibited control (Figure 5). Since TfR is largely concentrated within the clathrin-coated pits,[44] it is reasonable to see B6, which was explored as a TfR targeting peptide, mediate cellular import of nanoparticles via the clathrin-mediated endocytosis pathway. Cellular uptake of B6-NP was also inhibited by M-β-CD, which could selectively extract cholesterol and alter the structure of cholesterol-rich domains in cell membrane, suggesting that lipid raft-mediated pathway was involved as well. In the meanwhile, the internalization of B6-NP was reduced by monensin, confirming the involvement of lysosome in the intracellular transport of B6-NP. Taken together, we believed that B6-NP internalization in bEnd.3 cells was mediated by more than one cellular uptake mechanism, involving lipid raft-mediated endocytosis and clathrin-mediated endocytosis pathways.

In vitro cell viability analysis was conducted to evaluate the safety of B6-NP-NAP. As shown in Figure 6, no significant difference in cytotoxicity was observed between B6-NP-NAP and NP-NAP. Thus, B6-NP-NAP was regarded as a promising DDS without any significant cytotoxic effects on the cells tested.

A real-time biodistribution experiment was performed to study the B6-mediated brain targeting efficiency under an *in vivo* imaging system. A significant enhancement of the signal from B6-NP was observed during the 0.5−12 h experimental period compared with that from NP, indicating that B6, which present higher efficiency for brain accumulation, could be used as a potential brain targeting peptide. Further organ fluorescent images taken one hour post administration confirmed that the fluorescent signal of B6-NP in mouse brain was still much higher than that of NP (Figure 7B). In contrast, the accumulation of NP in liver, spleen, and lung might be attributed to its nonspecific capture by the mononuclear phagocyte system.

Animal models played a key role in the evaluation of therapeutics for AD.[45] Former studies showed that infusion of $A\beta_{1-40}$ led to AD-related spatial and nonspatial learning and memory deficits[46] and disruption of cholinergic function.[47] Models based on intracerebroventricularly injected Aβ allowed the evaluation of the neuroprotective effect of NAP toward toxicity associated with Aβ.[48] Moreover, coinjection of $A\beta_{1-40}$ with IBO induced enhanced neurotoxicity and provided a better model for studying the pathogenetic mechanisms leading to AD.[49] Therefore, in our study we chose mice intracerebroventricularly coinjected with preaggregated $A\beta_{1-40}$ and a small amount of IBO as AD model animal.

The MWM behavioral experiment and subsequently conducted biochemical indicators tests were applied to evaluate the NAP-related neuroprotection in AD model. Data from MWM test combined with determination of the activity of AChE (the enzyme that degrades acetylcholine) and ChAT (the enzyme that synthesizes acetylcholine) indicated that B6-NP-NAP significantly ameliorated the spatial learning deficit and cholinergic dysfunction even at the drug dose (0.02 μg) a quarter of that of NP-NAP (0.08 μg). Further HE staining was conducted to determine the difference in the cellular and microanatomical features between normal and injured brains. Consistent with former results, no visible damage was detected in the brain of mice treated with B6-NP-NAP even in a lower drug dose (0.02 μg) compared to other formulations. In contrast, NAP solution groups (0.02 μg and 0.08 μg) failed to produce any significant enhancement in either behavior study or AChE/ChAT activity test. This could result from the rapid degradation of NAP after *in vivo* injection. Overall, the findings here offered robust evidence that B6-NP might provide a more efficacious brain drug delivery system than unmodified NP and solution. Significantly enhanced neuroprotection effect of NAP against the learning impairments,[12] loss of cholinergic functions,[12] and loss of hippocampal neurons[50] induced by coinjection of $A\beta_{1-40}$ with IBO was achieved by B6-functionalized DDS.

■ CONCLUSION

In this study, we proposed B6-modified PEG-PLA nanoparticles as an effective DDS in mediating NAP transport into the brain following tail vein administration in mice. The resulting B6-NP exhibited significantly enhanced cellular accumulation/uptake over that of NP via lipid raft-mediated endocytosis and clathrin-mediated endocytosis pathway. *In vivo* imaging showed that B6-NP exhibited a desirable biodistribution profile with significantly enhanced accumulation in the brain. In the pharmacodynamic experiment, B6-NP-NAP treatment showed excellent amelioration in learning impairments, cholinergic disruption and loss of hippocampal neurons in AD model mice. These results definitely indicated that B6-NP might serve as a promising DDS to facilitate the transport of neuropeptides across the BBB to exert their therapeutic effect in the CNS.

AUTHOR INFORMATION

Corresponding Author

*Tel.: +86-21-51980066; fax: +86 21 51980069. E-mail: chenjun@fudan.edu.cn.

Author Contributions

First two authors contributed equally to this work.

Notes

The authors declare no competing financial interest.

ACKNOWLEDGMENTS

This work was supported by National Natural Science Foundation of China (81072592), National Key Basic Research Program (2010CB529800), National Science and Technology major Project (2012ZX09304004), Program for New Century Excellent Talents in University, Grants from Shanghai Science and Technology Committee (11430702200, 12ZR1416300 and 12 nm0502000), Innovation Program of Shanghai Municipal Education Commission (12ZZ107) and SJTU Funding (AE4160003).

REFERENCES

(1) Cacciatore, I., Baldassarre, L., Fornasari, E., Mollica, A., and Pinnen, F. (2012) Recent advances in the treatment of neurodegenerative diseases based on GSH delivery systems. *Oxid. Med. Cell Longev. 2012*, 240146.

(2) Povova, J., Ambroz, P., Bar, M., Pavukova, V., Sery, O., Tomaskova, H., and Janout, V. (2012) Epidemiological of and risk factors for Alzheimer's disease: a review. *Biomed. Pap. Med. Fac. Univ. Palacky Olomouc Czech Repub. 156*, 108−114.

(3) Feng, Y., and Wang, X. (2012) Antioxidant therapies for Alzheimer's disease. *Oxid. Med. Cell Longev. 2012*, 472932.

(4) Bassan, M., Zamostiano, R., Davidson, A., Pinhasov, A., Giladi, E., Perl, O., Bassan, H., Blat, C., Gibney, G., Glazner, G., Brenneman, D. E., and Gozes, I. (1999) Complete sequence of a novel protein containing a femtomolar-activity-dependent neuroprotective peptide. *J. Neurochem. 72*, 1283−1293.

(5) Gozes, I., Divinski, I., and Piltzer, I. (2008) NAP and D-SAL: neuroprotection against the beta amyloid peptide (1−42). *BMC Neurosci. 9* (Suppl3), S3.

(6) Matsuoka, Y., Jouroukhin, Y., Gray, A. J., Ma, L., Hirata-Fukae, C., Li, H. F., Feng, L., Lecanu, L., Walker, B. R., Planel, E., Arancio, O., Gozes, I., and Aisen, P. S. (2008) A neuronal microtubule-interacting agent, NAPVSIPQ, reduces tau pathology and enhances cognitive function in a mouse model of Alzheimer's disease. *J. Pharmacol. Exp. Ther. 325*, 146−153.

(7) Gozes, I., Zaltzman, R., Hauser, J., Brenneman, D. E., Shohami, E., and Hill, J. M. (2005) The expression of activity-dependent neuroprotective protein (ADNP) is regulated by brain damage and treatment of mice with the ADNP derived peptide, NAP, reduces the severity of traumatic head injury. *Curr. Alzheimer Res. 2*, 149−153.

(8) Ashur-Fabian, O., Segal-Ruder, Y., Skutelsky, E., Brenneman, D. E., Steingart, R. A., Giladi, E., and Gozes, I. (2003) The neuroprotective peptide NAP inhibits the aggregation of the beta-amyloid peptide. *Peptides 24*, 1413−1423.

(9) Zemlyak, I., Furman, S., Brenneman, D. E., and Gozes, I. (2000) A novel peptide prevents death in enriched neuronal cultures. *Regul. Pept. 96*, 39−43.

(10) Beni-Adani, L., Gozes, I., Cohen, Y., Assaf, Y., Steingart, R. A., Brenneman, D. E., Eizenberg, O., Trembolver, V., and Shohami, E. (2001) A peptide derived from activity-dependent neuroprotective protein (ADNP) ameliorates injury response in closed head injury in mice. *J. Pharmacol. Exp. Ther. 296*, 57−63.

(11) Wilkemeyer, M. F., Chen, S. Y., Menkari, C. E., Brenneman, D. E., Sulik, K. K., and Charness, M. E. (2003) Differential effects of ethanol antagonism and neuroprotection in peptide fragment NAPVSIPQ prevention of ethanol-induced developmental toxicity. *Proc. Natl. Acad. Sci. U. S. A. 100*, 8543−8548.

(12) Gozes, I., Giladi, E., Pinhasov, A., Bardea, A., and Brenneman, D. E. (2000) Activity-dependent neurotrophic factor: intranasal administration of femtomolar-acting peptides improve performance in a water maze. *J. Pharmacol. Exp. Ther. 293*, 1091−1098.

(13) Adessi, C., and Soto, C. (2002) Converting a peptide into a drug: strategies to improve stability and bioavailability. *Curr. Med. Chem. 9*, 963−978.

(14) Wong, H. L., Chattopadhyay, N., Wu, X. Y., and Bendayan, R. (2010) Nanotechnology applications for improved delivery of antiretroviral drugs to the brain. *Adv. Drug Delivery Rev. 62*, 503−517.

(15) Biddlestone-Thorpe, L., Marchi, N., Guo, K., Ghosh, C., Janigro, D., Valerie, K., and Yang, H. (2012) Nanomaterial-mediated CNS delivery of diagnostic and therapeutic agents. *Adv. Drug Delivery Rev. 64*, 605−613.

(16) Krol, S. (2012) Challenges in drug delivery to the brain: Nature is against us. *J. Controlled Release 164*, 145−155.

(17) van Rooy, I., Mastrobattista, E., Storm, G., Hennink, W. E., and Schiffelers, R. M. (2011) Comparison of five different targeting ligands to enhance accumulation of liposomes into the brain. *J. Controlled Release 150*, 30−36.

(18) Staquicini, F. I., Ozawa, M. G., Moya, C. A., Driessen, W. H., Barbu, E. M., Nishimori, H., Soghomonyan, S., Flores, L. N., Liang, X., Paolillo, V., Alauddin, M. M., Basilion, J. P., Furnari, F. B., Bogler, O., Lang, F. F., Aldape, K. D., Fuller, G. N., Hook, M., Gelovani, J. G., Sidman, R. L., Cavenee, W. K., Pasqualini, R., and Arap, W. (2011) Systemic combinatorial peptide selection yields a non-canonical iron-mimicry mechanism for targeting tumors in a mouse model of human glioblastoma. *J. Clin. Invest. 121*, 161−173.

(19) Visser, C. C., Stevanovic, S., Voorwinden, L. H., van Bloois, L., Gaillard, P. J., Danhof, M., Crommelin, D. J., and de Boer, A. G. (2005) Targeting liposomes with protein drugs to the blood-brain barrier in vitro. *Eur. J. Pharm. Sci. 25*, 299−305.

(20) Huwyler, J., Wu, D., and Pardridge, W. M. (1996) Brain drug delivery of small molecules using immunoliposomes. *Proc. Natl. Acad. Sci. U. S. A. 93*, 14164−14169.

(21) Lo, S. L., and Wang, S. (2008) An endosomolytic Tat peptide produced by incorporation of histidine and cysteine residues as a nonviral vector for DNA transfection. *Biomaterials 29*, 2408−2414.

(22) Nie, Y., Schaffert, D., Rodl, W., Ogris, M., Wagner, E., and Gunther, M. (2011) Dual-targeted polyplexes: one step towards a synthetic virus for cancer gene therapy. *J. Controlled Release 152*, 127−134.

(23) Ishihara, T., Kubota, T., Choi, T., Takahashi, M., Ayano, E., Kanazawa, H., and Higaki, M. (2009) Polymeric nanoparticles encapsulating betamethasone phosphate with different release profiles and stealthiness. *Int. J. Pharm. 375*, 148−54.

(24) Olivier, J. C. (2005) Drug transport to brain with targeted nanoparticles. *NeuroRx 2*, 108−19.

(25) Gao, X., Tao, W., Lu, W., Zhang, Q., Zhang, Y., Jiang, X., and Fu, S. (2006) Lectin-conjugated PEG-PLA nanoparticles: preparation and brain delivery after intranasal administration. *Biomaterials 27*, 3482−3490.

(26) Olivier, J. C., Huertas, R., Lee, H. J., Calon, F., and Pardridge, W. M. (2002) Synthesis of pegylated immunonanoparticles. *Pharm. Res. 19*, 1137−1143.

(27) Yu, D. H., Lu, Q., Xie, J., Fang, C., and Chen, H. Z. (2010) Peptide-conjugated biodegradable nanoparticles as a carrier to target paclitaxel to tumor neovasculature. *Biomaterials 31*, 2278−2292.

(28) Gao, X., Wang, T., Wu, B., Chen, J., Chen, J., Yue, Y., Dai, N., Chen, H., and Jiang, X. (2008) Quantum dots for tracking cellular transport of lectin-functionalized nanoparticles. *Biochem. Biophys. Res. Commun. 377*, 35−40.

(29) D'Hooge, R., and De Deyn, P. P. (2001) Applications of the Morris water maze in the study of learning and memory. *Brain Res. Brain Res. Rev. 36*, 60−90.

(30) Li, J., Huang, H., Miezan, E. J., Gao, X. L., Massicot, F., Dong, C. Z., Heymans, F., and Chen, H. Z. (2007) Pharmacological profile of

PMS777, a new AChE inhibitor with PAF antagonistic activity. *Int. J. Neuropsychopharmacol. 10*, 21−29.
(31) Kabanov, A. V., and Gendelman, H. E. (2007) Nanomedicine in the diagnosis and therapy of neurodegenerative disorders. *Prog. Polym. Sci. 32*, 1054−1082.
(32) Liu, Y., Huang, R., Han, L., Ke, W., Shao, K., Ye, L., Lou, J., and Jiang, C. (2009) Brain-targeting gene delivery and cellular internalization mechanisms for modified rabies virus glycoprotein RVG29 nanoparticles. *Biomaterials 30*, 4195−4202.
(33) Boado, R. J., Zhang, Y., Zhang, Y., Xia, C. F., Wang, Y., and Pardridge, W. M. (2008) Genetic engineering, expression, and activity of a chimeric monoclonal antibody-avidin fusion protein for receptor-mediated delivery of biotinylated drugs in humans. *Bioconjugate Chem. 19*, 731−739.
(34) Pardridge, W. M. (2008) Re-engineering biopharmaceuticals for delivery to brain with molecular Trojan horses. *Bioconjugate Chem. 19*, 1327−1338.
(35) Zhou, Q. H., Lu, J. Z., Hui, E. K., Boado, R. J., and Pardridge, W. M. (2011) Delivery of a peptide radiopharmaceutical to brain with an IgG-avidin fusion protein. *Bioconjugate Chem. 22*, 1611−1618.
(36) Boado, R. J., Zhang, Y., Zhang, Y., Xia, C. F., and Pardridge, W. M. (2007) Fusion antibody for Alzheimer's disease with bidirectional transport across the blood-brain barrier and abeta fibril disaggregation. *Bioconjugate Chem. 18*, 447−455.
(37) Boado, R. J., Hui, E. K., Lu, J. Z., and Pardridge, W. M. (2013) IgG-enzyme fusion protein: pharmacokinetics and anti-drug antibody response in rhesus monkeys. *Bioconjugate Chem. 24*, 97−104.
(38) Gabathuler, R. (2010) Approaches to transport therapeutic drugs across the blood-brain barrier to treat brain diseases. *Neurobiol. Dis. 37*, 48−57.
(39) Zhang, P., Hu, L., Yin, Q., Zhang, Z., Feng, L., and Li, Y. (2012) Transferrin-conjugated polyphosphoester hybrid micelle loading paclitaxel for brain-targeting delivery: synthesis, preparation and in vivo evaluation. *J. Controlled Release 159*, 429−434.
(40) Ulbrich, K., Hekmatara, T., Herbert, E., and Kreuter, J. (2009) Transferrin- and transferrin-receptor-antibody-modified nanoparticles enable drug delivery across the blood-brain barrier (BBB). *Eur. J. Pharm. Biopharm. 71*, 251−256.
(41) Huang, R. Q., Qu, Y. H., Ke, W. L., Zhu, J. H., Pei, Y. Y., and Jiang, C. (2007) Efficient gene delivery targeted to the brain using a transferrin-conjugated polyethyleneglycol-modified polyamidoamine dendrimer. *FASEB J. 21*, 1117−1125.
(42) Moos, T., and Morgan, E. H. (2000) Transferrin and transferrin receptor function in brain barrier systems. *Cell Mol. Neurobiol. 20*, 77−95.
(43) Gaillard, P. J., Voorwinden, L. H., Nielsen, J. L., Ivanov, A., Atsumi, R., Engman, H., Ringbom, C., de Boer, A. G., and Breimer, D. D. (2001) Establishment and functional characterization of an in vitro model of the blood-brain barrier, comprising a co-culture of brain capillary endothelial cells and astrocytes. *Eur. J. Pharm. Sci. 12*, 215−222.
(44) Nichols, B. (2003) Caveosomes and endocytosis of lipid rafts. *J. Cell Sci. 116*, 4707−4714.
(45) Van Dam, D., and De Deyn, P. P. (2006) Drug discovery in dementia: the role of rodent models. *Nat. Rev. Drug Discovery 5*, 956−970.
(46) Olariu, A., Yamada, K., Mamiya, T., Hefco, V., and Nabeshima, T. (2002) Memory impairment induced by chronic intracerebroventricular infusion of beta-amyloid (1−40) involves downregulation of protein kinase C. *Brain Res. 957*, 278−286.
(47) Nag, S., Yee, B. K., and Tang, F. (1999) Reduction in somatostatin and substance P levels and choline acetyltransferase activity in the cortex and hippocampus of the rat after chronic intracerebroventricular infusion of beta-amyloid (1−40). *Brain Res. Bull. 50*, 251−262.
(48) Matsuoka, Y., Gray, A. J., Hirata-Fukae, C., Minami, S. S., Waterhouse, E. G., Mattson, M. P., LaFerla, F. M., Gozes, I., and Aisen, P. S. (2007) Intranasal NAP administration reduces accumulation of amyloid peptide and tau hyperphosphorylation in a transgenic mouse model of Alzheimer's disease at early pathological stage. *J. Mol. Neurosci. 31*, 165−170.
(49) Ito, Y., Ito, M., Takagi, N., Saito, H., and Ishige, K. (2003) Neurotoxicity induced by amyloid beta-peptide and ibotenic acid in organotypic hippocampal cultures: protection by S-allyl-L-cysteine, a garlic compound. *Brain Res. 985*, 98−107.
(50) Zemlyak, I., Manley, N., Sapolsky, R., and Gozes, I. (2007) NAP protects hippocampal neurons against multiple toxins. *Peptides 28*, 2004−2008.